An Automatic Detection Method for Liver Lesions Using Abdominal Computed Tomography

Sheng-Fang Huang
Department of Medical Informatics
Tzu Chi University
Hualien, Taiwan
SFhuang@mail.tcu.edu.tw

Kuo-Hsien Chiang
Department of Radiology
Buddhist Tzu Chi General Hospital
Hualien, Taiwan
spider0645@mail.tcu.edu.tw

Treatments for liver cancer requires the information of liver such as its boundary, precise size and localization of tumors, and spatial relations among these tissues. A computer-aided diagnosis (CAD) system can to help doctors conveniently acquire the information and provide valuable second opinions. In our study, we aim to developing a fully automatic method for detecting liver tumors using abdominal CT images. The proposed method consists of three modules. First, a DICOM image was read and preprocessed using an adaptive liver window to enhance its contrast. Then we used statistical and morphological features to extract the liver mass. Finally, we extracted texture features for each pixel in the extracted liver regions and applied neural network to classify pixels and to identify whether they were belonged to normal tissues or liver lesions. In order to validate the proposed study, we have tested our method in a database from 50 liver patients. We demonstrated the accuracy of the tumor segmentation method using a cross-validation protocol and three area error metrics. The performance was evaluated using TP, FP, and FN percentages, which were 71.82%, 37.83% and 28.17%.

Keywords-abdominal computed tomography (CT); liver lesion; computer-aider diagnosis (CAD);image segmentation; nueral network (NN)

I. INTRODUCTION

Planning a liver intervention is usually a challenging task for a surgeon [1]. However, by using imaging technology, medical decisions of liver tissue pathology can be portrayed with various medical imaging modalities such as ultrasonography (US), computed tomography (CT), or magnetic resonance imaging (MRI). Among them, CT is considered the most robust imaging technique for the detection of liver lesions, such as hepatocellular [2]. Furthermore, the success of modern and future liver interventions also relies on a computer-aided diagnosis (CAD) systems that can assist doctors to carry out surgical planning and simulations [3].

Any kind of liver local treatment requires the information for liver such as its contour, precise size and localization of tumors, accurate liver vessel topography, and spatial relations among these tissues. Thus, an objective and reproducible method to detect liver tumors would be profitable for clinical use. Moreover, such an approach should also work for various tumor types and can avoid multiple and successive segmentations. Nevertheless, such a task is quite difficult due to the ambiguities of brightness changes between normal tissues and tumors. A striking resemblance usually exists between abnormal and normal tissues. At image level, tumors could have diverse intensities and appearances within healthy liver tissues and become less distinguishable. Another challenging problem is due to the liver itself, since it contains a high level of vascularization, and therefore, the acquired images could therefore become noisy.

We would like to address the problems both on liver segmentation and the detection of liver lesions using abdominal CT images. The proposed CAD system was based on neural network technique. In our study, we initially used the liver window to enhance the contrast of the input image. A sequence of morphological operations was then applied to find the contours for ribcage and liver. Next, a texture analysis was performed to extract statistical features for each pixel of the liver. Finally, we used these features as inputs for neural network to classify tumor pixels within the liver region. The rest of this paper is organized as follows. We show the detailed steps for the proposed method in Section III, which consists of three subsections to describe the details of preprocessing, liver segmentation, and texture analysis. In Section IV, we present the results and statistical analysis for

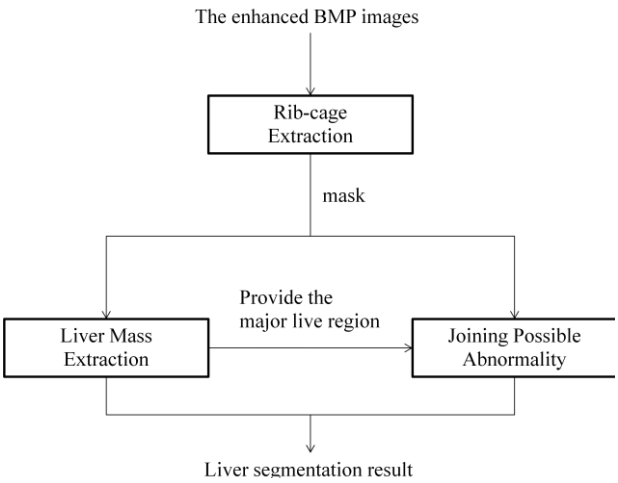

Figure 1. Flowchart of liver segmentation.

our method. Finally, we make discussion and conclusions in Section V.

II. DATA AQUISITION

The dataset included abdominal CT images acquired from 50 patients, with each patient averagely having 30 images. Totally, 1500 DICOM images were used in our study. Each CT image was was scanned at an interval of 5 mm. The technique of 300 mAs was used with 120 KVP, field of Vision we can achieve image enhancement to highlight he-

(fov) 280. The dimension of image matrix was 512 x 512. For each patient, 100cc of omnipaque 350 was injected intravenously at the rate of 3cc per second. Scanning delay was 30 seconds, where 20 second spiral scanning was used with a pitch of 0.984. We assumed that the liver located on the left of the abdomen for all the input images.

III. METHOD

A. *Image Enhancement*

Pixels in a CT image are displayed in terms of relative radio-density. The pixel itself can be quantified according to the mean attenuation of the tissues. The Hounsfield unit (HU) scale, which ranges from -1024 to +3071, is measured by a linear transformation of original linear attenuation coefficients in a material. Using liver window level, patic lesion brightness. Liver windows have a window level equal to the attenuation levels of hepatic parenchyma (50 HU without contrast material; 100 HU after the intravenous administration of contrast material) and a narrower window width (150 HU) than conventional soft-tissue window levels. However, medical images differ in every body and every taking. A fixed liver window may not result in a good enhancement for liver and liver lesions. In our study, we computed an adaptive threshold value as window center to solve the problem. Since liver is located on the left side of the abdomen according our scanning protocol, we computed the mean of pixels which have HU values ranging from 0 HU to 300 HU in the left-half of the input image as the new window center. The window width was determined by experiments. A small window width can enhance details of liver compositions, but could also increase the amount of other irregular patterns, such as noise. In our study, the window width was chosen 150.

B. *Liver segmentation*

Our liver segmentation method consists of several steps as shown in Figure 1, which we will describe the details in the following sections.

1) *Rib-cage Extraction*

The infiltration of fat content lowers the HU values in human liver. A fatty liver could become less distinguishable when it neighbors upon the extra-abdominal fat closely, which may induce an erroneous segmentation result. Because the extra-abdominal fat locates outside the rib cage, we can find the location of ribs and draw a contour to exclude the fat.

First, the initial CT scan image was thresholded using values ranging from 0 to 300 HU to obtain the body periphery. A center R was then determined by the spatial center of the body region. The boundary for body can therefore be represented by its signature, denoted by $s(\theta)$, which is a 1-D function that describes the distant from R for a specific angle θ. Next, it is necessary to compute the signature $r(\theta)$ for rib cage so that we can evaluate the size

of structuring element for the erosion by subtracting $r(\theta)$ from $s(\theta)$ for any θ.

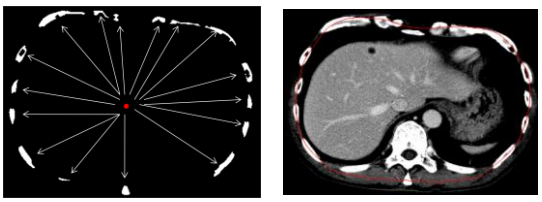

(a) (b)

Figure 2. The steps for obtaining rib-cage contour.

TABLE I. CRITERIA FOR FOUR DEFINED CATEGORIES.

	Thresholding (gray value)	***RS* (pixel)**	***RHW***	***RA***	***RL***
Category 1	0-0.8σ	>100	>0.4	>0.35	>1.6
Category 2	0-30	>100	>0.6	>0.6	>0.5
Category 3	10- (ū-1.2σ)	>100	>0.7	>0.5	>0.9
Category 4	25- (ū-1.2σ)	>100	>0.5	>0.4	>1.3

We computed $r(\theta)$ according to the locations of rib bones. Initially, the image enhanced by liver window was thesholded using gray level values of 230. Next, we used morphological operations (opening using a structuring element with diameter of 7) to eliminate small unwanted irregularities, such as noise and the hospital bed. The largest region and any other regions locating in a distance less than ε were also removed because they may be resulted from spine bones and liver vascularity. In our study, the value of ε was given by 0.6 times of the maximum distance among all $r(\theta)$. For the regions left, we computed the length from *R* to each pixel in these regions. The value of $r(\theta)$ was assigned by the average length for each θ. Since rib bones do not form a connected contour for the rib cage, we calculated the average $r(\theta)$, denoted by m_r, and its standard deviation σ_r to adjust the values of $r(\theta)$, For some θ where $r(\theta)$ is not in the range of $m_r \pm \sigma_r$, $r(\theta)$ will be replaced by m_r. Additionally, for each θ, we recomputed $r(\theta)$ using median and average filtering within ± 17° for obtaining a smooth contour. Figure 2 describes the process in this section.

2) *Contour Extraction for Liver*

The mass of liver consists of two parts: normal liver tissues and the abnormalities induced by liver cancer. The normal liver can be obtained simply by thresholding with new threshold values recomputed from the inside of the extracted ribcage. Given the enhanced gray scale image as input, we first filtered out pixels with gray levels equal to 0 or larger than 200 within the rib-cage, since they could belonged to abdominal fat tissues or bones. We excluded them by assigning these pixels with 255. A median filer was then applied on the image to reduce the interference of noise. We recomputed the average $\bar{u}$, and its standard deviation σ within the left side of the image. The candidate pixels of liver was selected according to the range within $\bar{u} \pm 1.2\sigma$. Finally, we performed morphological operations of 3 closings to connect gaps, followed by 7 openings to separate from other organs or tissues. Finally, the largest region was chosen as the possible liver region.

Tumor masses show a distinct appearance in the liver. Compared to normal tissues, they usually have lower intensities, and could generate holes and caves in the liver region obtained from the previous thresholding procedure. Therefore, we must apply additional steps for detecting these parts to assemble a full liver mass. We defined four categories for different intensity ranges as shown in Table 1. A unique binary image B_p was generated for some category *p*. For every region *q* in B_p, we computed the smallest rectangle *R* enclosing *q*, and evaluated three shape features of *q*, as shown in (1) to (3), where *w* and *h* denote respectively the width and height of the rectangle. We specifically defined a set of criteria for each *p* to select regions in B_p. For each category, regions that satisfied its criteria were selected and joined to the liver mass.

$$RS = Area \quad of \quad q. \tag{1}$$

$$RHW = \min\{\frac{w}{h}, \frac{h}{w}\}. \tag{2}$$

$$RA = \frac{Area \quad of \quad q}{Area \quad of \quad R}. \tag{3}$$

$$RL = \frac{\text{Number of pixels neighnboring to liver mass}}{\text{Number of pixels NOT neighboring to liver mass}} \tag{4}$$

3) *Texture Analysis*

We require features to differentiate between normal liver tissue and hepatic lesions. Haralick texture features are generally used for image classification on abdominal CT [4,5]. The features are calculated based on the construction of a co-occurrence matrix. Suppose that a co-occurrence matrix P is used to describe the patterns of neighboring pixels in an image at a given distance *d*. In the calculation of texture

features, four co-occurrence matrices are necessary to describe different orientations, including P_0, P_{90}, P_{45}, and P_{135}, which respectively represent a co-occurrence matrix that describes pixels adjacent to one another in four directions. We computed Haralick texture features for every point where it has four co-occurrence matrices. Therefore, we summed them up to one matrix to calculate its statistical features. There were total 16 texture features computed for each liver pixel, including 13 Haralick textures and four local statistical features. The three local statistical features were normalized mean, local variance, local, and entropy The normalized mean was a ratio of local mean to global mean for liver region, because the gray level values for liver and liver lesions in a CT scan image vary in different patients. A normalized ratio would be better to capture the difference between normal liver and the abnormalities. However, not all the texture features were used for classification. After computing features for all pixels, we first evaluated their feasibility by using the unpaired Student's t-test (two -tailed) to evaluate and keep the feature that its t-test value under 0.01. The proposed features were statistically significant over the entire database and were used to classify pixels. In our study, only six features among the 16 texture features were chosen, including normalized mean, local variance, local entropy, Haralick entropy, Haralick energy, and Haralick sum of squares, which we used for tumor detection.

4) Neural Network

To identify whether a region is a normal liver tissue or liver lesions, we adopted a general multi-layered perceptron (MLP) neural network and chose the back-propagation algorithm as the learning rule. The value produced by the output node of the neural network lies between 0 and 1. The output value was used as a probability evaluation for the prediction of tumor regions. In the study, we used four layer back-propagation algorithms. The first layer was an input and included five neurons (nodes) that denote the foregoing six features. The framework of this neural network consisted of two hidden layers, with the number of neurons being given seven and three respectively, and the last layer was the output layer with two neurons which classifies the input pixels whether it is of tumor or of liver.

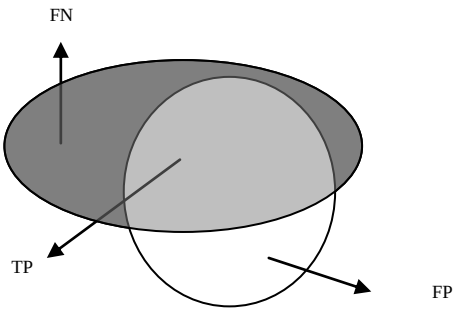

Figure 3. Areas for evaluating TP, FP, and FN rates.

In order to stabilize this neural network, we trained the data with 500 iterations. The learning parameter was set 0.01 and the momentum was chosen as 0.01 for converging quickly.

IV. Experiment Results

The *k*-fold cross-validation method was used to estimate the accuracy of feature classification. With the k-fold cross-validation method, the 50 case were randomly divided into *k* groups. The first group was chosen as test set, and the remaining (*k*-1) groups were used as train set for training the neural network. The trained model produced by the network was then used to test the former group that we left aside. The process repeated until every group has been tested. Each time when a group was to be tested, the other (k-1) groups were used to train the network first. In our study, *k* was 5. A trial is predicted right if the tumor region can be successfully selected.

To evaluate the accuracy of our segmentation, we quantitatively compared the automated results with the liver lesions. In order to measure the performance of the proposed segmentation method, we used three different error measures. They were true-positive (TP), false-positive (FP) and negative-positive volume fractions, which were defined as follows [6].

$$TP = \frac{A_a \cap A_n}{A_m} \quad (5)$$

$$FP = \frac{|A_a \cup A_m - A_m|}{A_m} \quad (6)$$

$$FN = \frac{|A_a \cup A_m - A_a|}{A_m} \quad (7)$$

where the term A_m refers to the area of the tumor determined by manual segmentation and A_a is the area of the lesion determined by the proposed

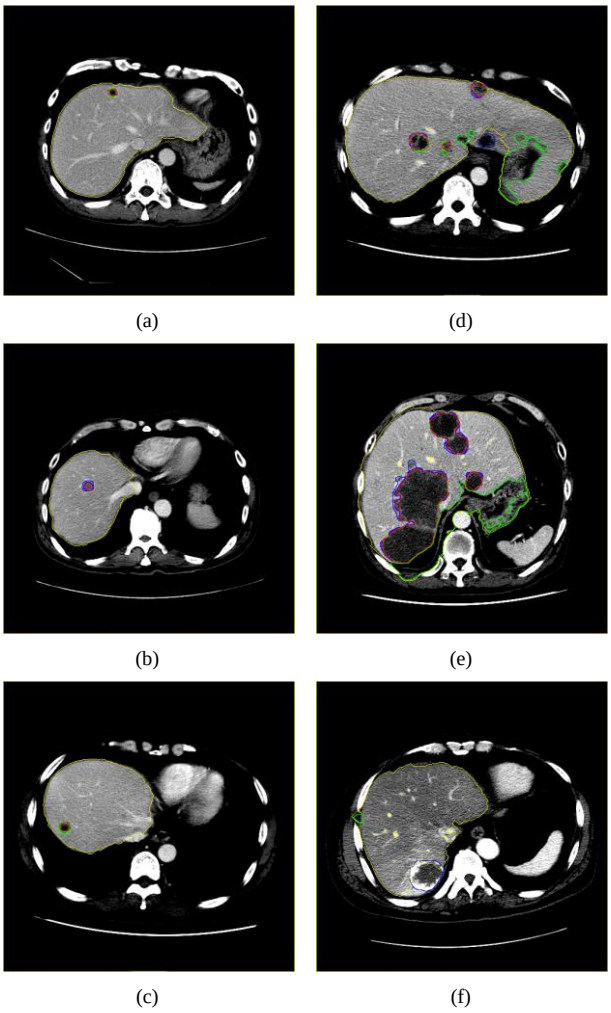

Figure 4. Segmentation results for liver and tumors using the proposed method (the red indicates TP. the blue FN, and the green FP area).

method. Ideally, a good segmentation results in higher TP with FP and FN being relatively low. Figure 3 shows the area corresponding to TP, FP and FN. In our study, the average TP, FP, and FN percentages were 71.82%, 37.83% and 28.17%. Figure 4 shows some examples of the final results for our proposed method. The cases displayed in Figures 4 (a)-(c) show better results, where the corresponding TP rates are 98.39%, 88.64%, and 99.28%, and FP rates 1.6%, 0%, and 0.7%. On the other hand, the cases displayed in Figures 4 (d)-(f) are examples that results in erroneous segmentation, where the corresponding TP rates are 67.33%, 89.76%, and 0%, and FP rates 77.98%, 41.96%, and 100%.

V. Discussions and Conclusions

In this paper, we present a fully automated segmentation system requiring no human intervention to segment tumor areas on abdominal CT images. It can portray the structural information of liver lesions to surgeons for further diagnosis. In our study, the average TP, FP, and FN percentages were 71.82%, 37.83% and 28.17%. However, there are also limitations in our method. Due to the various structures of liver lesions, it is challenging for us to determine a region whether it is a tumor region or a background region if it locates between hepatic resection. Any faulty contour in the liver segmentation could therefore lead to erroneous detection results. In some cases, we observed that the TP rates drop when the tumor in question locates closely to the boundary of liver or blood vessels, so therefore it may be excluded as early as in the step of liver segmentation. In addition, if a tumor is too small, our system could also fail to detect its existence. So far, we used shape features and statistical evaluation to address this problem. In the future, we aim at improving the performance of segmentation by selecting reference image from continuous abdominal CT images. Moreover, we will reform the method of liver lesion segmentation by incorporating with more features. Furthermore, we will use contour tracking method to improve the edge of liver lesions segmentation.

References

[1] V. Sojar, D. Stanisavljevic, M. Hribenrnik, M. Glusic, D. Kreuh, U. Velkrah, T. Fius, “Liver surgery training and planning in 3D virtual space,” Int. Congr. Ser., vol. 1268, pp. 390–394, 2004.

[2] H. M. Taylor and P. R. Ros, “Hepatic imaging: An overview,” Radiologic Clinics of North America, vol. 36, no. 2, 1998.

[3] JB. Fasquel, V. Agnus, J. Moreau, L. Soler, J. Marescaux, “An interactive medical image segmentation system based on the optimal management of regions of interest using topological medical knowledge,” Comput. Methods Programs Biomed., vol. 82, pp. 213–230, 2006.

[4] Miltiades Gletsos, Stavroula G. Mougiakakou, George K. Matsopoulos, Konstantina S. Nikita, Alexandra S. Nikita, Dimitrios Kelekis, “A Computer-Aided Diagnostic System to Characterize CT Focal Liver Lesions: Design and Optimization of a Neural Network Classifier,” IEEE Trans. Information Technology in Biomedicine, vol. 7, no. 3, September 2003.

[5] John E. Koss, F. D. Newman, T. K. Johnson, D. L. Kirch, “Abdominal Organ Segmentation Using Texture Transforms and a Hopfield Neural Network.” IEEE Trans. Medical Imag., vol. 18, no. 7, July 1999.

[6] A madabhushi and D.N. Metaxas, “Combining low-, high-level and empirical domain knowledge for automated segmentation of ultrasonic breast lesions,” IEEE Trans. Medical Imag., vol. 22, no. 2, pp.155-169, February, 2003.